Journal of Structural Dynamics, Special issue on Tribomechadynamics, (pp. 88-104) 2024
Can real-time flange tightness monitoring be possible with strains? A numerical pre-study.

Journal of Structural Dynamics

Can real-time flange tightness monitoring be possible with strains? A numerical pre-study.

W. Witteveen *[1], S. Desch[2], and L. Koller[2]

[1] *Upper Austria University of Applied Sciences, Degree Program Mechanical Engineering, Roseggerstraße 15, 4600 Wels, Austria*
[2] *FH OOE Forschungs und Entwicklungs GmbH, Roseggerstraße 15, 4600 Wels, Austria*

Abstract

The tightness of a flange depends on the current deformation state of the structure. For obvious reasons, this could be a critical and important information. In this paper, numerical preliminary investigations are presented on the question whether the deformation state inside a contact surface can be estimated in a very short time with a few strain measurements outside the contact surface.The presented theory is numerically evaluated using a flange with 12 bores. It turns out, that the deformation inside the contact area, and therefore the tightness, can be computed out of strain data in milliseconds. The magnitude of the strains are in a measurable range and the numerical results show robustness against noise. Even if the presented approach may not be applicable one-to-one for measurements, this numerical preliminary investigation shows that mechanical strains could in principal be used to observe the state or the tightness within a joint.

Keywords: Flanges, tightness, deformation of contact surfaces, strain gauges, condition monitoring

Received on July 25, 2024, *Accepted on October 14, 2024*, *Published on October 22, 2024*

1 Introduction

Bolted joints are an important design element and very common in mechanical engineering. Flanges, which can be used to connect pipes, are a relevant example. Often, such flange connections must also be "tight" so that the media flowing through the pipes does not escape. Loads and vibrations cause deformations in the flange and these deformations obviously affect the tightness. In the worst case, the deformations become so large that the tightness is no longer guaranteed and the system leaks. In addition to the economic damage, this scenario also poses a potential danger to people. The possibility of monitoring leak tightness of flanges in real-time can therefore be a critical improvement to such systems.

Within the contact area of a joint, highly complex processes occur. Depending on the deformation state of the structure, the contact in any area of the joint can be either closed or open. In the closed case, both contact surfaces can slip or stick relative to each other. If the deformation state of the structure is time-dependent, then all of these states can occur at different times in different areas of the joint. The gap or pressure distribution in the contact area are numerically easy to compute but very challenging to measure experimentally. Numerical studies suggesting such complex behavior have existed for some time. For example, reference can be made to section 4.1 of Lenz's dissertation (Lenz [1]) from 1997 or Kontoleon et al. [2] from 1999 (in particular figures 7 and 8). Both publications use the finite element method, which leads to accurate results in case of fine meshing but high computing times. In order to also enable the consideration of dynamic effects (=vibrations), the method from Pichler et al. [3] works with trial vectors (so called contact modes) for describing the deformations of the joint. In Witteveen et al. [4], this method was verified by a qualitative comparison with measurements. In all cases, it can be seen how complex the conditions

*wolfgang.witteveen@fh-wels.at

in the contact area develop and change over time. The possibilities for experimentally determining the global effects of contact and friction are manifold. For example, effects such as mode coupling, amplitude-dependent damping and natural frequencies can be measured. Three representative examples can be found in Wall et al. [5], Daouk et al. [6] and Bournine et al. [7]. To our knowledge, there is no documented method to compute a field variable like the gap distribution or flange tightness from this information. For the direct experimental determination of the complex gap or pressure distribution in the contact area, we are aware of three methods. One option is a static pressure film which can be clamped between the contacting surfaces. After the pressure has been applied, the bolts must be loosened again, the film is removed and the color change indicates the magnitude of the pressure. Such films are suitable for assessing the pressure and gap distribution according to the bolt load, but not for permanent monitoring. An application where a computed pressure distribution is compared to a measured one can be found in figure 24 of Jewell et al. [8]. The second option is the use of a paste (known as Engineer's blue), see Li and Chan [9]. This paste is applied inside the contact area and the involved materials have to be transparent. The color of the paste changes due to the local pressure. This information is tracked with a camera and then used to calculate the acting pressure and the gap distribution. The necessary transparency of the components is already a knockout criterion for monitoring the contact status of any practically relevant structure. The third and last option is a certain foil which is used in Dreher et al. [10]. This foil is clamped between the contact surfaces. The sensor is based on a material whose electrical properties are pressure-dependent. The foil is divided into cells and the contact pressure can be determined for each individual cell. Dreher et al. [10] provides a principal confirmation of the complex changes of the pressures inside the contact area due to structural vibrations. In principle, this technology seems to be suitable for contact and leak monitoring, but there are some disadvantages: (1) Since the foil has to be clamped, the behavior of the joint changes. (2) It is questionable how pressure and heat resistant the foil is - important questions for practical use. (3) Another question is whether such films can be used for very large flanges, such as those required for pipes with a diameter of 1m. Condition monitoring of bolt preload and the detection of bolt looseness should be mentioned as an active field of research. Various methods are used to determine the loss of preload in a bolt. This is of no direct importance in the present work as its goal is the real-time reconstruction of the current gap in the contact zone. Of course, the change in the gap can also be used to draw conclusions about the bolt preload. However, this issue is not addressed in this paper. As a starting point for research in the direction of "bolt looseness detection" reference is made to the publications of Chelimilla et al. [11] and Tong et al. [12]. In He et al. [13] a strategy for determining the tightness of a flange under the influence of temperature changes is presented. The current temperature field is reconstructed via measured temperatures. The reconstructed temperature field is then used to perform a Finite Element Analysis to determine the contact pressure in the gasket. The paper does not provide any specific information on the real-time capability of the method. Vibrations (which take place on a completely different time scale) are not taken into account. Several publications deal with the behaviour of flanges when they deform. Examples are Khan et al. [14], Zhu et al. [15], [16] and [17]. This is always about gaining fundamental knowledge and insight. Monitoring a flange in real time is not an issue.

This purely numerical feasibility study explores the principal possibility of real-time monitoring the contact and tightness condition of a flange with any geometry on the basis of known strains. The aim of this work is a kind of numerical proof-of-concept that with a few strains measured outside the joint, the state inside the joint can be estimated. In this work, this hypothesis is verified by reconstructing the gap distribution in a joint via a few strain values. The gap distribution was selected as it provides the most comprehensive and complex result data. This data can then be utilized for calculating pressure and assessing the level of tightness. If this is possible with numerical data and a certain stability is given (e.g. against noise), then it may also work on real structures for less complex but more practically relevant questions such as "Is the flange in a critical state regarding tightness?". The focus of this paper is not on developing a method directly applicable to real-world structures. This publication aims to numerically demonstrate that it is feasible to extract information about the joint state using a few number of strain gauges.

This publication is organized as follows: Section 2 explains the theory. A virtual and model-based sensor is presented that can reconstruct the gap distribution in a joint very precisely with the resolution of the Finite Element (FE) mesh using just a few strain gauge sensors. In section 3 the theory is applied to a numerical example and demonstrates its feasibility in principle. It deals with two pipes connected by a flange with 12 bores. The pipe is loaded by external forces. A non-linear computation is used as a reference. It is shown that with few virtual strain gauge sensors the deformation state in the contact area can excellently be reconstructed. At the end of section 3 some comments are given with respect to the magnitude of the strains and the results robustness against noise. In the concluding section, the results are critically discussed, some improvements and an outlook is given.

2 Theory

2.1 Brief notes on DEIM and POD

In the further course of this work, the Discrete Emperical Interpolation Method (DEIM) and Proper Orthogonal Decomposition (POD) are used. These methods are discussed in detail in the literature, which is why only their basic idea and some literature references are given here.

2.1.1 DEIM

DEIM will be used in this work for the optimal determination of S strain measurement locations out of $\bar{S}$ potential ones. This brief explanation is therefore based on strains. It is assumed that a $(\bar{S} \times 1)$ vector $\bar{\boldsymbol{\varepsilon}}$ holds all potential available strains of a structure. Furthermore it is assumed that this vector can be computed by a linear superposition of S vectors $\bar{\boldsymbol{\varepsilon}}_{B,1}$ to $\bar{\boldsymbol{\varepsilon}}_{B,S}$ which are stored column-wise in the matrix $\bar{\boldsymbol{E}}_B$. As outlined in section 2.1.2, POD allows to compute such a matrix based on snapshots. If $S < \bar{S}$, then DEIM offers a possibility for the computation of $\bar{\boldsymbol{\varepsilon}}$ on the base of a subset of measurements represented by the $(S \times 1)$ vector $\boldsymbol{\varepsilon}$. The fact that $\boldsymbol{\varepsilon}$ holds a subset of sensors in $\bar{\boldsymbol{\varepsilon}}$ can mathematically be expressed as

$$\boldsymbol{\varepsilon} = \boldsymbol{B}^T \bar{\boldsymbol{\varepsilon}} \tag{1}$$

with the $(S \times \bar{S})$ matrix $\boldsymbol{B}^T$ which has only one unit-entry per row. Based on the matrix $\bar{\boldsymbol{E}}_B$, the DEIM algorithm returns this matrix $\boldsymbol{B}^T$ (and thus the selection of sensors) together with a $(\bar{S} \times S)$ matrix $\bar{\boldsymbol{E}}$ so that

$$\bar{\boldsymbol{\varepsilon}} = \bar{\boldsymbol{E}} \boldsymbol{\varepsilon} \tag{2}$$

with

$$\bar{\boldsymbol{E}} = \bar{\boldsymbol{E}}_{\boldsymbol{B}} (\boldsymbol{B}^T \bar{\boldsymbol{E}}_{\boldsymbol{B}})^{-1} \tag{3}$$

More detailed information can be found in the original publication of Chaturantabut and Sorensen [18] or in the work of Tiso and Rixen [19]. Note that DEIM can also be applied in the case when the number of columns in $\bar{\boldsymbol{E}}_B$ is not equal to the number of entries in $\boldsymbol{\varepsilon}$ (= number of sensors). In that case the matrix inversion of the former equation becomes a pseudo inverse, see chapter 12 of the doctoral thesis of Rutzmoser [20]. The application of DEIM will be denoted further on as

$$(\boldsymbol{B}^T, \bar{\boldsymbol{E}}) = DEIM(\bar{\boldsymbol{E}}_B, S) \tag{4}$$

with S being the number of final strain measurements (which is equal to the number of entries in $\boldsymbol{\varepsilon}$ and number of rows in $\boldsymbol{B}^T$).

2.1.2 POD

In this paper, POD is used to compute a base $\bar{\boldsymbol{E}}_B$ for DEIM. Again, all explanations are based on strains. Given are T $(\bar{S} \times 1)$ vectors $\bar{\boldsymbol{\varepsilon}}_{T,1}$ to $\bar{\boldsymbol{\varepsilon}}_{T,T}$ which are stored column-wise in the matrix $\bar{\boldsymbol{E}}_T$. These data are called snapshots or training data and can be obtained by measurements or simulations. The reasonable assumption is made that more training data are available as potential sensors, i.e. $T > \bar{S}$. POD of rank S computes S $(\bar{S} \times 1)$ vectors $\bar{\boldsymbol{\varepsilon}}_{B,1}$ to $\bar{\boldsymbol{\varepsilon}}_{B,S}$ which can be used as a base for the approximation of the space of all training data. This base has the property, that the reconstruction of all training data is optimal in the Euclidean sense. In this work the application of POD is denoted as

$$(\boldsymbol{\lambda}, \bar{\boldsymbol{E}}_B) = POD(\bar{\boldsymbol{E}}_T, S) \tag{5}$$

where the $(\bar{S} \times S)$ matrix $\bar{\boldsymbol{E}}_B$ holds the S base vectors $\bar{\boldsymbol{\varepsilon}}_{B,1}$ to $\bar{\boldsymbol{\varepsilon}}_{B,S}$ in its columns. POD uses a singular value decomposition which delivers as a result singular values. They are called proper orthogonal values (POV) in the context of POD. The first S POV are stored into the $(S \times 1)$ vector $\boldsymbol{\lambda}$ and sorted in descending order. The magnitude of an entry of $\boldsymbol{\lambda}$ correlates with the importance of the corresponding base vector for the approximation of the training data space.

There is a huge number of POD related publications available and a starting point for more detailed investigations concerning POD can be Chatterjee [21] and Kerschen and Golinval [22].

2.2 Contact modes

Efficient dynamics of FE structures requires model order reduction because nodal degrees of freedom would lead to far too many equations. Model order reduction via projection approximates a $(N \times 1)$ vector $\boldsymbol{x}$ of nodal displacements (or rotations) in the form of

$$\boldsymbol{x} = \boldsymbol{\Phi}\boldsymbol{q} \tag{6}$$

where the $(N \times Q)$ matrix $\boldsymbol{\Phi}$ holds Q trial vectors in its columns. These trial vectors are scaled by Q scaling factors which are collected in the $(Q \times 1)$ vector $\boldsymbol{q}$. The trial vectors are commonly called "modes" and the scaling factors "modal coordinates". More information on model order reduction via projection can be found in chapters 3 and 4 of the doctoral thesis of Rutzmoser [20]. Two groups of modes must be considered in order to obtain useful solutions for the problem at hand. Therefore, the matrix $\boldsymbol{\Phi}$ is subdivided into

$$\boldsymbol{\Phi} = \begin{bmatrix} \boldsymbol{\Phi}_G & \boldsymbol{\Phi}_C \end{bmatrix} \tag{7}$$

where the submatrix $\boldsymbol{\Phi}_G$ holds common modes, like the famous one of Craig and Bampton [23]. These modes can capture global deformations quiet well but are not suitable for an accurate representation of the local deformations inside a contact zone which is required for the problem under consideration. These local deformations can be captured by so-called contact modes which are collected in the columns of the submatrix $\boldsymbol{\Phi}_C$. For this work it is sufficient to know that the mode base just presented is able to represent all relevant deformations accurately enough, including those in the contact area. There is sufficient literature on the computation and validation of contact modes available. The publication of Pichler et al. [24] is a good starting point for the interested reader. The following assumptions are now made for all further considerations: (1) Both contact surfaces belong to the same body. They are therefore in self-contact and the deformations of both surfaces are described by corresponding lines of $\boldsymbol{\Phi}$. (2) There is small sliding contact between the surfaces. This is a common assumption for bolt connections. (3) For simplicity it is assumed, that both contact surfaces are congruently meshed with C node-to-node contact pairs. Note, that the former mentioned contact modes are just valid in the presence of assumption (1) and (2). Based on these assumptions the relative normal displacement of the two contact surfaces can be computed by a single matrix vector multiplication in the form

$$\boldsymbol{g} = \boldsymbol{\Phi}_n\boldsymbol{q} \tag{8}$$

where the $(C \times 1)$ vector $\boldsymbol{g}$ holds the normal distance of all C node-to-node contact pairs. The $(C \times Q)$ matrix $\boldsymbol{\Phi}_n$ can be formed out of $\boldsymbol{\Phi}$, more details can be found in section 4.1 in Pichler et al. [24]. The C relative displacements of the contact nodes in both tangential directions are collected in the $(C \times 1)$ vectors $\boldsymbol{z}_1$ and $\boldsymbol{z}_2$ and can be computed along

$$\boldsymbol{z}_j = \boldsymbol{\Phi}_{t,j}\boldsymbol{q} \tag{9}$$

with $j = 1, 2$. The $(C \times Q)$ matrices $\boldsymbol{\Phi}_{t,1}$ and $\boldsymbol{\Phi}_{t,2}$ can again be computed based on $\boldsymbol{\Phi}$, see section 4.2 in Pichler et al. [24].

2.3 Gap reconstruction based on strain data

It is assumed that $\bar{S}$ strains can potentially be measured. These are stored in the $(\bar{S} \times 1)$ vector $\bar{\boldsymbol{\varepsilon}}$. In the case of linear strains, there is a linear relationship between the nodal displacements and the strains. Consequently the strains depend linearly on the modal coordinates $\boldsymbol{q}$ and can be given as

$$\bar{\boldsymbol{\varepsilon}} = \bar{\boldsymbol{E}}_B\boldsymbol{q} \tag{10}$$

with a $(\bar{S} \times Q)$ matrix $\bar{\boldsymbol{E}}_B$ which can be constructed based on $\boldsymbol{\Phi}$. A simple way to do this is to measure the distance between two FE nodes and divide it by the initial distance. This is not numerically exact, but probably comes closer to the behaviour of a real strain gauge, which also has a finite expansion, than if the strain at each point is determined with the help of the FE trial functions.

If the strains are known, the pseudo inverse can be used to compute $\boldsymbol{q}$ out of $\bar{\boldsymbol{\varepsilon}}$ with

$$\boldsymbol{q} = \bar{\boldsymbol{E}}_B^{\dagger}\bar{\boldsymbol{\varepsilon}} \tag{11}$$

Here, the pseudo inverse is a potential critical operation if fewer strains are available than modal coordinates are to be determined- this will be remembered again later. If relation (11) is plugged into (8), the gap (and thus the tightness) can be determined with

$$\boldsymbol{g} = \bar{\boldsymbol{G}}\bar{\boldsymbol{\varepsilon}} \tag{12}$$

where the $(C \times \bar{S})$ matrix $\bar{\boldsymbol{G}}$ can be computed along

$$\bar{\boldsymbol{G}} = \boldsymbol{\Phi}_n \bar{\boldsymbol{E}}_B^{\dagger} \tag{13}$$

Remember that the overbar describes a quantity which is based on all potential available strain measures. A very high number of measurements - say several hundred - may be theoretically possible, but it is not practical. In the next two subsections we look at the question of how to get a good result with as few sensors as possible.

2.3.1 Sensor selection without training data

When the number of available strains $\bar{S}$ is higher than the number of modes Q, it seams reasonable, that a sufficient result quality can be obtained by S sensors, where $S \approx Q$. For this reduction process the columns of $\bar{\boldsymbol{E}}_B$ can be considered as a kind of artificial training data when the according modal coordinate in $\boldsymbol{q}$ is set to one and all others to zero. The application of DEIM

$$(\boldsymbol{B}_1^T, *) = DEIM(\bar{\boldsymbol{E}}_B, S) \tag{14}$$

delivers $\boldsymbol{B}^T$ which holds the DEIM - optimal collection of S sensors out of the $\bar{S}$ available. The interpolation matrix denoted as $\bar{\boldsymbol{E}}$ in equation (4) is not needed here. A left hand side multiplication of equation (10) with $\boldsymbol{B}_1^T$ delivers

$$\boldsymbol{\varepsilon} = \boldsymbol{E}\boldsymbol{q} \tag{15}$$

where $\boldsymbol{\varepsilon} = \boldsymbol{B}_1^T \bar{\boldsymbol{\varepsilon}}$ and $\boldsymbol{E} = \boldsymbol{B}_1^T \bar{\boldsymbol{E}}_B$. If the transformations from equations (11) to (13) are carried out in a similar way starting with (15) one obtains

$$\boldsymbol{g} = \boldsymbol{G}_1 \boldsymbol{\varepsilon} \tag{16}$$

where the $(C \times S)$ matrix $\boldsymbol{G}_1$ can be computed along

$$\boldsymbol{G}_1 = \boldsymbol{\Phi}_n \boldsymbol{E}^{\dagger} \tag{17}$$

Due to the properties of the pseudo inverse, it can be expected, that the results are meaningful as long as S is approximately Q and not much smaller. In the case of lets say 10 modes, this may be feasible. However, if the joint becomes more complex, then 100 or perhaps 200 modes may be necessary to describe the deformations in the contact area accurately enough. In such a case the expected number of strain gauges is not practical to handle anymore.

2.3.2 Sensor selection with training data

It is assumed that T training data in the form of $(\bar{S} \times 1)$ vectors $\bar{\boldsymbol{\varepsilon}}_{T,1}$ to $\bar{\boldsymbol{\varepsilon}}_{T,T}$, which are stored column-wise in the matrix $\bar{\boldsymbol{E}}_T$, are available. The application of POD (see equation (5))

$$(\boldsymbol{\lambda}, *) = POD(\bar{\boldsymbol{E}}_T, T) \tag{18}$$

delivers a vector $\boldsymbol{\lambda}$ holding all available singular values. The decrease of the singular values is a measure of how many base vectors are necessary for a reliable subspace. Let us assume that S trial vectors are sufficient for such a base which now can be obtained by

$$(\boldsymbol{\lambda}, \bar{\boldsymbol{E}}_B) = POD(\bar{\boldsymbol{E}}_T, S) \tag{19}$$

The optimal sensor placement can now be computed by the application of DEIM

$$(\boldsymbol{B}_2^T, \boldsymbol{E}_B) = DEIM(\bar{\boldsymbol{E}}_B, S) \tag{20}$$

If

$$\bar{\boldsymbol{\varepsilon}} = \boldsymbol{E}_B \boldsymbol{\varepsilon} \tag{21}$$

is inserted in (12) the gap can be reconstructed with

$$\boldsymbol{g} = \boldsymbol{G}_2 \boldsymbol{\varepsilon} \tag{22}$$

where the $(C \times S)$ time invariant matrix $\boldsymbol{G}_2$ can be computed along

$$\boldsymbol{G_2} = \bar{\boldsymbol{G}} \boldsymbol{E}_B \tag{23}$$

Note that the dimension of $\boldsymbol{G}_2$ is independent of the number of modes. It is only important that the potential sensors are more than the modes. The number of sensors depends on the size of the basis which is necessary to describe the space of the training data. As usual with trained systems, this approach will fail, if a state occurs, that cannot be approximated by the training data.

2.4 Additional comments on the methods characteristics and real-time capability

In the theory section two methods have been introduced. One method needs no training data and the second one does. The numerical investigations in section 3 underline an assumption already made in the theory section, namely, that only the approach with training data will lead to an acceptable number of sensors. Therefore, just this method is commented in the following subsections.

2.4.1 Possible flow

As the purpose of this work is a fundamental examination of the question "Is it possible to draw conclusions about the contact situation from a few strains outside the contact", the flow is only given very roughly. There are certainly still unanswered questions (like calibration) regarding the measurement. However, this work provides a preliminary investigation on whether it makes sense to think concretely about measurements at all.

1. Find optimal sensor positions $\boldsymbol{B}_2^T$ and compute matrix $\boldsymbol{G}_2$ with a model of the structure.
2. Apply strain gauges at the positions denoted by $\boldsymbol{B}_2^T$.
3. Start measurement. For each time instant:
   (a) Get strain data from strain gauge sensors via data acquisition system.
   (b) Compute gap via the matrix vector multiplication in equation (22).

2.4.2 Comments on the matrix vector multiplication in equation (22)

The matrix vector multiplication of equation (22) is the key point of the method. The strains are transformed into the gap of the joint using a simple matrix vector multiplication. No contact or friction laws are analysed. Instead, one measured set of deformations (= strains) is used to compute another set of deformations (= gap). This is only possible because information from a numerical model have been used.

Note that the dimensions of the matrix $\boldsymbol{G}_2$ do not depend on the number of modes. It is possible to use a high number of modes and contact modes in order to improve the accuracy without loosing any efficiency. The efficiency only depends on the number of entries in $\boldsymbol{g}$ and the number of strain gauges.

The reconstruction itself does not depend on any kind of contact laws, friction laws and related parameters. All contact forces occur naturally on a real structure and lead to corresponding strains and deformations in the contact area. The strains are then used to reconstruct these deformations. This leads to the requirement that the contact situation must be represented accurately enough in the training data. Since the training data are generated with simulations, the specific contact law and friction law do play a role there.

Table 1: CPU time for the computation of the gap due to strains

Number of entries in **g**	1000	1000	1000	1000
Number of strain gauges	10	50	100	200
Number of entries in G_2	10000	50000	100000	200000
CPU Time for one Matrix Vector Multiplication in [s]	1,55E-06	8,44E-06	1,15E-05	1,12E-04

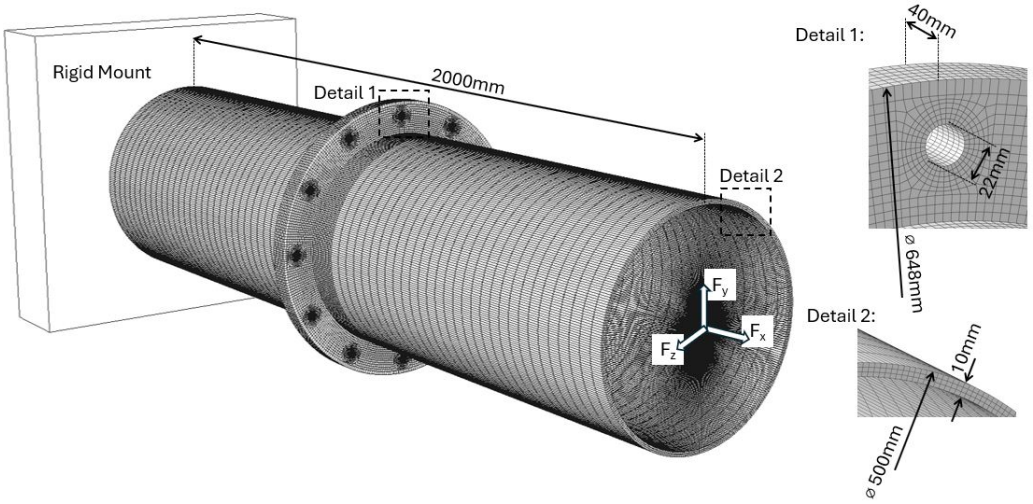

Fig. 1: FE model of a pipe structure with a flange

2.4.3 Comments on the real-time capability

Real-time capability requires that in an actual realisation, step 3.b of the flow chart in section 2.4.1 is significantly faster than the sampling time of the data acquisition system. As emphasised several times, this step involves a simple matrix vector multiplication according to equation (22).

In order to estimate the duration of this operation, matrix $\boldsymbol{G}_2$ was created with different dimensions and random numbers. The multiplication in equation (22) was performed 10000 times with each matrix. The strain vector was also filled with random numbers. This task has been performed using MATLAB on a Windows 10 laptop with the following parameters: Intel(R) Core(TM) i7-8650U CPU @ 1.90GHz 2112 MHz, 4 Core(s), 8 Logical Processor(s), 32 GB RAM. The measured times for one multiplication can be taken from table 1.

As will be confirmed in the numerical example, the first column (10 virtual strain gauges) is the most relevant. But even if the second column (50 virtual strain gauges) is still included, the necessary time is less than 0.01ms. If a similar time is estimated for step 3.c in the above flow, then the state of the flange should be observable in the millisecond range.

3 Numerical feasibility study: Flange with 12 bores

The proposed method is tested on a purely numerical example. The aim is to numerically verify the above theory that the deformation state of a joint, and thus the tightness, can be determined with sufficient accuracy using just a few strain gauge measurements. Only if the numerical verification is successful it will make sense to think about an application of this method or a modified one to a real structure in the future.

3.1 The structure

As shown in Fig. 1, two pipes are connected with a flange. The pipes have an outer diameter of 500mm and a wall thickness of 10mm. Each of the two flanges has a thickness of 20mm and an outer diameter of 648mm. The total length of the FE model from end to end is 2000mm. The 12 bores have a diameter of 22mm, which corresponds to M20 screws. The entire structure is rigidly mounted on one side and 3 forces can be applied on the other side. These forces (F_x, F_y and F_z) are collected in the (3×1) vector $\boldsymbol{f}_L$. For this purpose, the nodes of the outermost surfaces

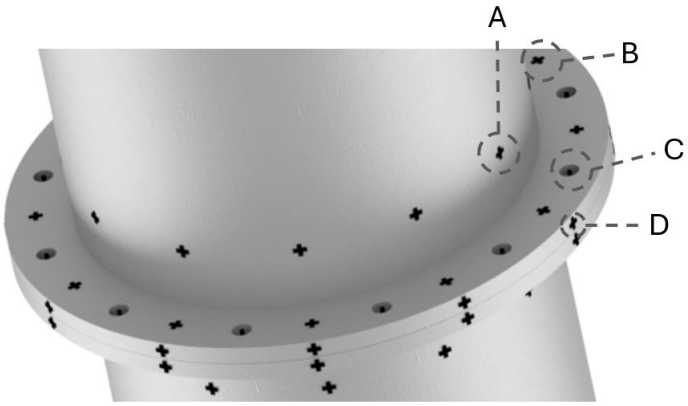

Fig. 2: Flange area with all potential strain gauges

were pulled together with a kinematic coupling to a node in the middle. Where the bolt heads would touch the flange surface, all FE nodes are pulled together with a distributed coupling to a center node. A bolt load is realized by pulling the two middle nodes of a bore together with a force. The FE model consists of 131040 linear hexahedron elements and 179162 nodes. The contact surfaces of the flange are congruently meshed with 7944 ($= C$) node pairs. The contact pressure p_i of node pair number i ($1 \leq i \leq C$) is computed by the simple nonlinear penalty law

$$p_i = \begin{cases} 0 & g_i \geq 0 \\ k_n g_i & g_i < 0 \end{cases} \tag{24}$$

where g_i holds the distance (=gap) of the i-th node pair and k_n represents the penalty stiffness (Unit: N/mm^3). The nodal force f_i is obtained by

$$f_i = A_i p_i \tag{25}$$

where A_i is the associated area of node pair i. The tangential stresses in the directions 1 and 2 of the contact plane $\tau_{j,i}$ ($j = 1, 2$ and $1 \leq i \leq C$) are computed along

$$\tau_{j,i} = \begin{cases} 0 & g_i \geq 0 \\ z_{j,i} k_t |g_i| / g_0 & (g_i < 0)\ \&\ (g_0 > |g_i| > 0) \\ z_{j,i} k_t & (g_i < 0)\ \&\ (|g_i| \geq g_0) \end{cases} \tag{26}$$

where $z_{j,i}$ holds the tangential displacement in direction j and k_t a tangential penalty factor (Unit: N/mm^3). The parameter g_0 defines a penetration limit for a linear scaling of the friction force in order to avoid discontinuities. Compared to the friction models discussed in Porter et al. [25] and Porter and Brake [26] this contact law is rather non-physical. Remember, that the aim of this work is the reconstruction of the gap inside a joint based on strain gauge measurements. To successfully demonstrate this goal, the actually chosen friction law plays no role. The former simple friction model was chosen to accelerate the non-linear computation for the generation of test and training data. The tangential nodal forces are computed out of the tangential stress analog to equation (25). The parameters mentioned above were defined for this study as k_n =20000N/mm^3, k_t =60000N/mm^3 and g_0 =0.0001mm.

Fig. 2 shows the positions of all potential strain measurements. The potential sensors can be roughly divided into four groups. In Fig. 2 one exemplary sensor of each group is marked. Group A contains sensors on the surface of the pipe next to the flange. The sensors of group B are mounted on the surface of the flange ring. Group C stands for strain gauges applied inside a bolt to measure the longitudinal elongation. Such bolts can be purchased commercially. The strain gauges of group D are applied on the outer circumference of the flange ring. The sensors of groups A, B, and D are symmetrically arranged around the contact plane. Each potential sensor position from A, B, and C stands for two sensors, one for each surface direction. In total, there are 156 ($= \bar{S}$) potential sensor positions.

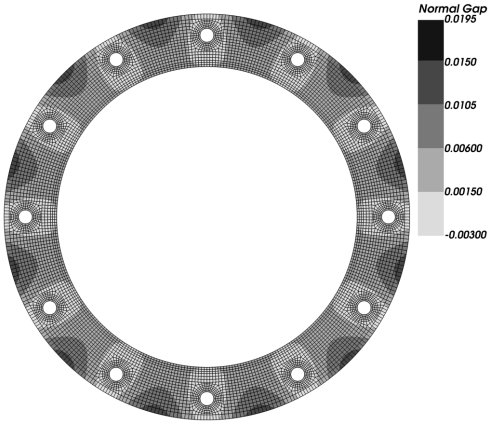

Fig. 3: Gap in the flange due to bolt load

3.2 Nonlinear Computation

The potential of the presented method is numerically tested on the basis of non-linear computations. The results of these non-linear computations are the normal distances in the contact area (=gap) as well as the strains at the sensor positions. Based on these strains, the gap in the joint is then reconstructed using the proposed method and then compared with the actual gap from this computation.

The non-linear equation on which the computations are based is

$$\boldsymbol{K}\boldsymbol{q} + \boldsymbol{f}_c = \boldsymbol{f} \tag{27}$$

with the $(Q \times Q)$ reduced stiffness matrix K, the $(Q \times 1)$ reduced vector of external forces $\boldsymbol{f}$ and the $(Q \times 1)$ reduced contact force vector $\boldsymbol{f}_c(g_i, z_{1,i}, z_{2,i})$. The index i ranges from 1 to C. The reduced quantities are obtained from the non-reduced one with $K = \boldsymbol{\Phi}^T \boldsymbol{K}_{FE} \boldsymbol{\Phi}$, $f = \boldsymbol{\Phi}^T \boldsymbol{f}_{FE}$ and $f_c = \boldsymbol{\Phi}^T \boldsymbol{f}_{FE,c}(g_i, z_{1,i}, z_{2,i})$. The subscript FE denotes a quantity in the context of the FE model. The contact kinematics $(g_i, z_{1,i}, z_{2,i})$ are computed out of the modal coordinates using equations (8) and (9). Equation (27) was solved with Matlab using the command fsolve(...). Standard settings were used. The mode base $\boldsymbol{\Phi}$ consists of 103 modes where 50 contact modes are included and the remaining modes are computed along the method of Craig and Bampton [23]. Some comments on the selected number of contact modes are given in the next subsection.

The fact that the investigation is based on non-linear statics is not a limitation of the generality. With the proposed method, strains measured at a point in time are converted into an instantaneous deformation state of the contact surfaces. Whether these strains come from a static or dynamic computation is not important. Static computations are more practical for this feasibility study, as they are easier and quicker to perform.

3.3 Bolt load

As mentioned above, at both ends of the flange bores, FE nodes were pulled together on a center node with a distributed coupling. These two nodes per bore were pressed together with 50kN. This leads to a maximum contact pressure of 57N/mm^2, see the right picture of Fig. 4. This is in the same range as the measured pressures in Dreher et al. [10]. The bolts could withstand a significantly higher load which would lead to a very similar distribution but higher pressures. The maximum penetration due to the penalty approach is -0.003mm which is considered to be sufficiently small. Fig. 3 shows the gap inside the flange according to the bolt load. The color scale was defined in such a way that a gap greater than 0.015mm is marked with black color which indicates critical opening. All values below are marked with some kind of grey color. The tolerance of 0.015mm is due to the assumption that a sealing compound has been lubricated between the contact surfaces and it compensates for minimal openings. The color bar does not change throughout this work. The contact due to bolt load which is shown in Fig. 3 is therefore tight and there is no area where the critical opening of 0.015mm is exceeded.

Fig. 4 shows the pressure inside the contact area with 50 contact modes (left picture) and with 150 contact modes (right picture). It can be seen, that the result with 50 contact modes is of good quality, even it is not fully converged. As the quality of the results is already very good and the effort for the many non-linear computations (see section 3.2) remains significantly lower, only 50 contact modes are used for this feasibility study. The use of even more contact modes plays a minor important role in this work for the following reasons:

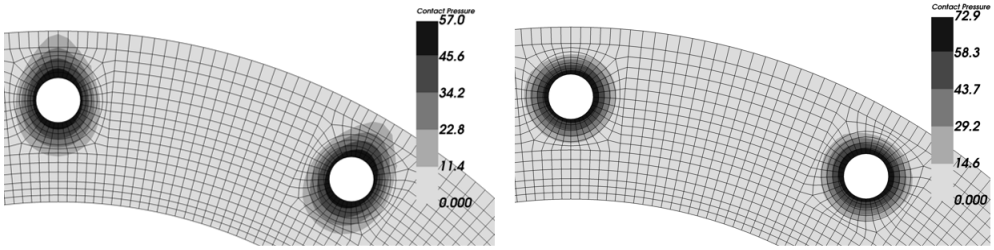

Fig. 4: Pressure [N/mm^2] in the flange due to bolt load with 50 contact modes (left picture) and 150 contact modes (right picture)

- The numerical example below confirms the assumption from section 2.3.1, that approximately as many strain gauges as modes are required for the approach without training data. For this and other reasons, which will be explained later, this approach is not practicable for real structures, regardless of whether 50 or 150 modes are used.
- As already emphasized in the introduction, the present work is a numerical preliminary investigation with regard to the feasibility of an implementation on real structures. Due to the measurement inaccuracies of the strain gauges alone, it will never be possible to obtain results as exact as those obtained here. The goal of a realistic application will therefore not be the exact reconstruction of the gap, but maybe the detection of a critical operating state with regard to tightness. This will be just as possible with 50 contact modes as with 150.
- In the method with training data (section 2.3.2), the selection of the strain gauge positions does not depend on the contact modes but on the content of the training data space. The reconstruction of the gap on the basis of these strain data is carried out with a matrix vector multiplication, see equation (22). The dimensions of the matrix do not depend on the number of contact modes, but their entries do. The more modes are used, the more accurate. For the reasons mentioned before, however, it seems questionable whether with real measurement data, which are also noisy, better results can be achieved with 150 contact modes than with 50 contact modes. This is certainly a question that would have to be investigated when working with real structures and measured strain data.

3.4 Test data

The test data are used to validate the method and are obtained by non-linear computations as explained in section 3.2. The gap distribution in the contact area is reconstructed using the strains and finally compared to the computed gap. As error measure for the gap a quantity e_i is defined as

$$e_i = \frac{|\boldsymbol{g}_i - \boldsymbol{g}_{NL,i}|}{|\boldsymbol{g}_{NL,i}|} 100\% \tag{28}$$

where the vector $\boldsymbol{g}_{NL,i}$ contains the gap of a load case with index i according to the non-linear reference computation and $\boldsymbol{g}_i$ the one of the reconstruction based on strain measurement. To summarize the errors of L load cases, the arithmetic mean value according to

$$e_m = \frac{1}{L} \sum_{i=1}^{L} e_i \tag{29}$$

is introduced.
The loads for the test data are computed along

$$\boldsymbol{f}_L = \begin{pmatrix} F_x 10^a \\ F_y 10^a \\ F_z 10^a \end{pmatrix} \tag{30}$$

where F_x, F_y and F_z are uniformly distributed random numbers between -1 and 1. For a proper consideration of higher and lower load levels in the test set, the symbol a takes on the values 6 and 4. The two values are varied so

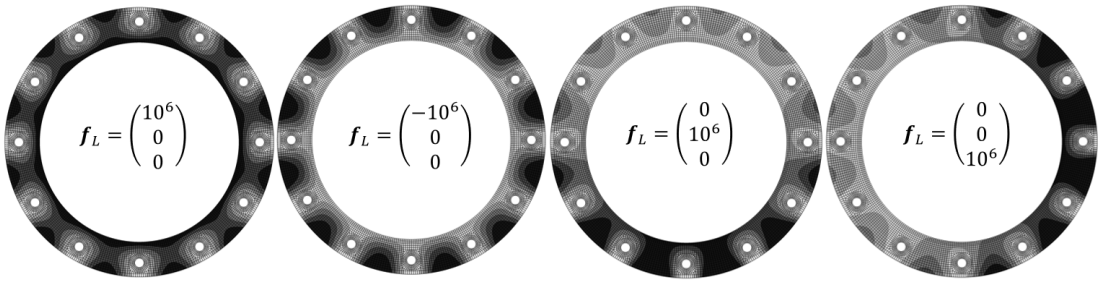

Fig. 5: Gap in the flange due to maximum loads in x, y and z direction

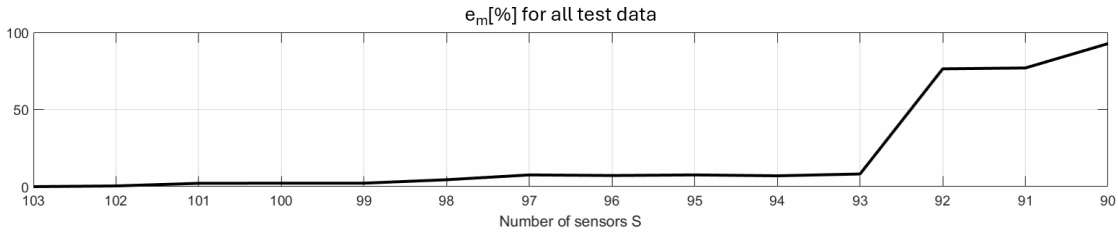

Fig. 6: Mean test data error for different number of sensors

that all possible combinations occur. With three rows, this results in 8 possibilities. Each of these eight possibilities is generated 15 times with different random numbers F_x, F_y and F_z. This results in 120 loads for 120 test sets.

To get an impression of the magnitude of the load, Fig. 5 shows the gap in the flange according to the maximum loads in the individual directions x, y and z. At maximum load in the longitudinal direction (= x), large areas already open above the critical value (marked in black). Leakage definitely occurs with the loads in the transverse directions (=y and z), as areas with critical gap reach continuously from the inside to the outside.

3.5 Numerical results for sensor selection without training data

In this section, the gap reconstruction is based on the formulas presented in section 2.3.1. As explained there, it can be expected, that the number of required sensors is approximately equal to the number of modes which are used to characterize the bodies deformation. Fig. 6 contains the mean errors of the 120 test sets (see equation (29)) for a decreasing number of sensors. The x-axis starts with 103 sensors and it can be seen that the mean error e_m over all test cases is almost zero. Further it can be seen that this error is still acceptable when the number of sensors is higher as 92 sensors. When the number of sensors is decreased to 92, the mean error of all test cases raises to a high value. This confirms the expectation, that the number of sensors is comparable to the number of modes.

What the increase in error actually means is illustrated in Fig. 7 using a specific test case. The leftmost image is the gap with 103 sensors where there is only a very small error. One can clearly see that the load leads to a gap on the left side (black color). The image with 93 sensors is still very similar, whereas with 92 sensors the situation changes significantly.

The investigations in this chapter produced the expected results. If no training data are used, then approximately as many sensors are required as there are modes. With a moderate number of modes, this may be a conceivable solution. However, if the joint becomes more complex, a large number of sensors are required, which makes this approach somewhat impractical. The situation can improve dramatically if training data is used to further minimize the number of sensors.

3.6 Numerical results for sensor selection with training data

In this section it is assumed that strain training data are available and the gap reconstruction is based on the formulas presented in section 2.3.2. The training data are generated similarly to the test data as explained in section 3.4, except that each of the eight variations of the exponent is generated 75 times with different random numbers. The strains due to these 600 load cases form the columns of the matrix $\bar{\boldsymbol{E}}_T$. The application of POD to this matrix gives singular values (=POV) as shown in Figure Fig. 8.

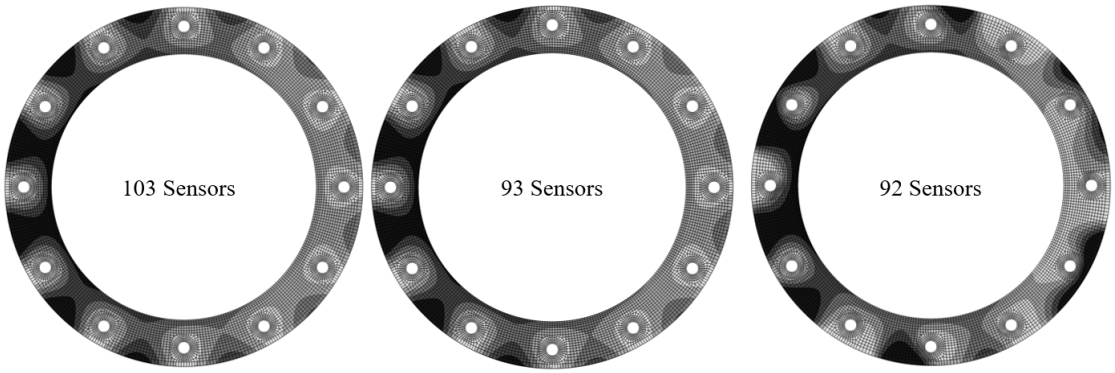

Fig. 7: Gap of one specific test case for different number of sensors

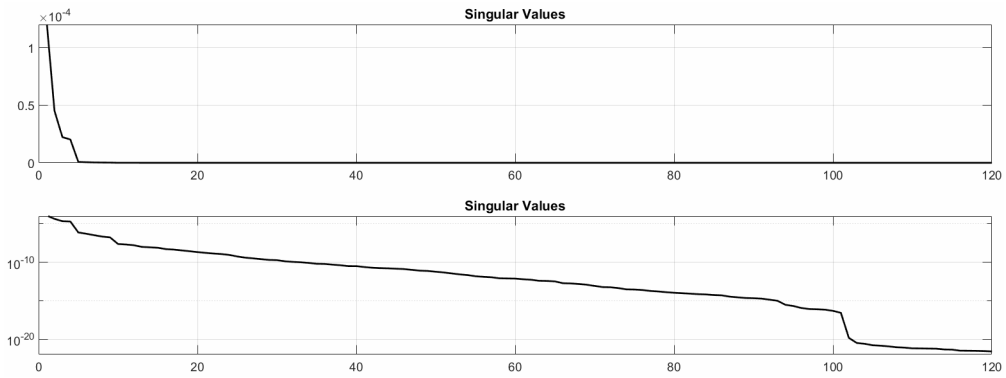

Fig. 8: POV of matrix $\bar{\boldsymbol{E}}_T$, linear and logarithmic plot

The POV drop very quickly, by a factor of 100,000 after 10 values. There is a very clear jump between number 103 and 104. This is to be expected, as the structure is described with 103 modes. However, the rapid drop at the beginning gives reason to believe that a very good result can be achieved with just a few sensors.

The mean error $e_m[\%]$ (see equation (29)) of all 120 test sets for different numbers of selected sensors is shown in Fig. 9. It can be seen that the error very quickly becomes relatively small. Based on this plot one could assume that 10 sensors will deliver an acceptable result.

Fig. 10 shows the error $e_i[\%]$ for 10 sensors and each test case. The largest error of 9.5% occurs with test data set number 96 which is a result of load $\boldsymbol{f}_L^T = (-380000\ 430000\ 510000)$. Fig. 11 reveals that this error of 9.5% for data set number 96 is acceptable small.

Fig. 12 shows all ten sensor positions. Two of the ten sensors are strain gauges that detect the longitudinal elongation of the bolts and belong to sensor group C (see Fig. 2). The other eight sensors belong to group B. Just strains in tangential direction have been selected. No sensor of group A and D has been considered.

In summary, it can be said that the number of sensors can be dramatically reduced if the possible strains can be represented by the superposition of few basis vectors. This is probably very often the case, since for one structure the

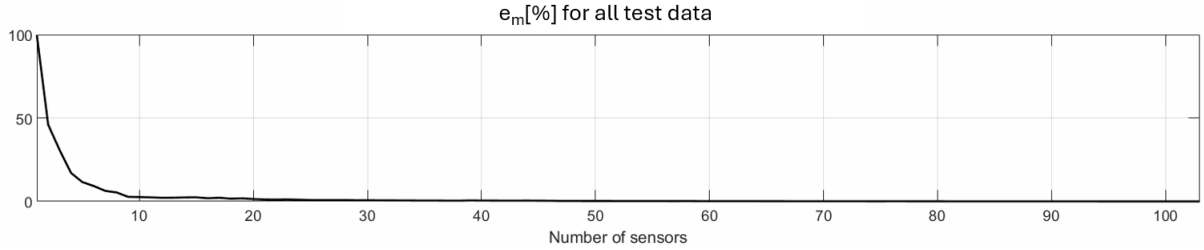

Fig. 9: Mean test data error for different number of sensors

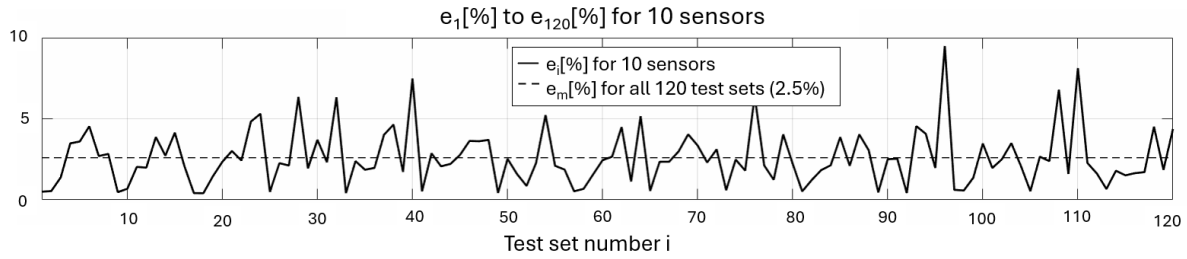

Fig. 10: Error $e_i[\%]$ for all test sets and 10 sensors

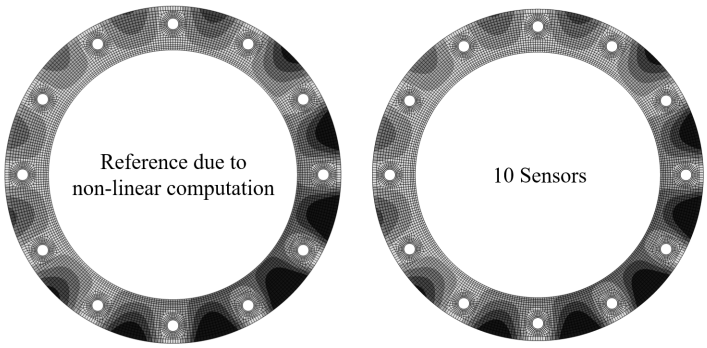

Fig. 11: Flange gap due to load case 96 for 10 sensors (right) and as result of the non-linear reference computation (left)

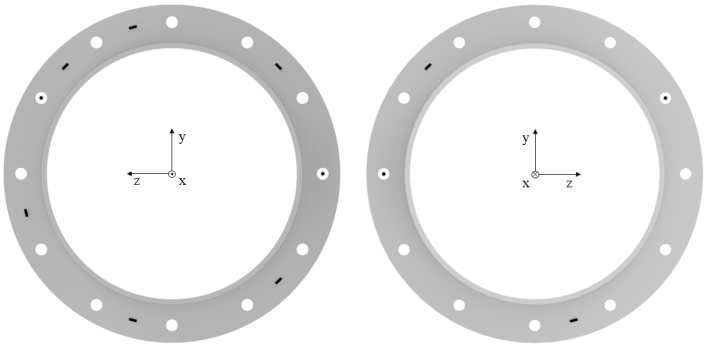

Fig. 12: Positions of the ten sensors

Table 2: Magnitude of the strains

	Sensor 1 (Bolt)	Sensor 2 (Bolt)	Sensor 3	Sensor 4	Sensor 5	Sensor 6	Sensor 7	Sensor 8	Sensor 9	Sensor 10
Bolt Load	9,92E-04	9,92E-04	2,74E-05	2,71E-05	2,75E-05	2,72E-05	2,71E-05	2,70E-05	2,60E-05	2,57E-05
Fx=1E+6	9,99E-04	1,00E-03	2,58E-04	2,64E-04	2,58E-04	2,59E-04	2,64E-04	2,62E-04	-1,75E-04	-1,78E-04
Fx=-1E+6	9,93E-04	9,94E-04	-1,34E-04	-1,35E-04	-1,34E-04	-1,34E-04	-1,35E-04	-1,35E-04	2,52E-04	2,49E-04
Fy=1E+6	1,00E-03	9,94E-04	-6,20E-05	-4,89E-05	6,90E-05	1,94E-04	1,50E-04	-4,95E-05	-4,05E-05	8,19E-05
Fz=1E+6	1,01E-03	1,02E-03	-1,13E-05	-4,86E-05	-6,12E-05	-8,08E-06	1,47E-04	1,49E-04	5,88E-05	-2,22E-05
Loadcase 96	1,01E-03	9,85E-04	-8,02E-05	-8,74E-05	-7,10E-05	-4,64E-06	5,95E-05	-3,77E-05	1,02E-04	1,13E-04

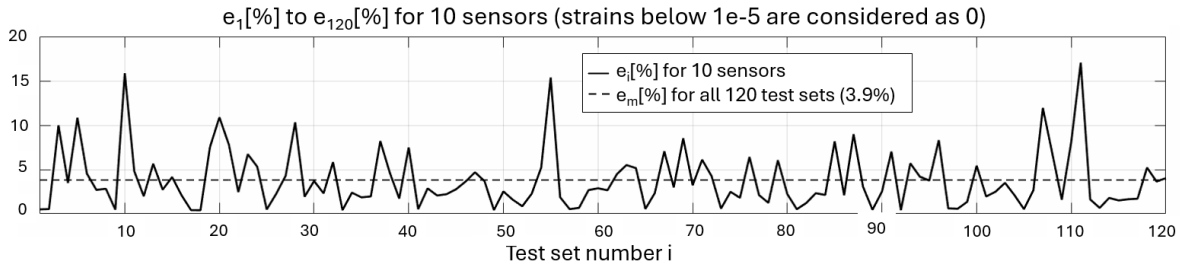

Fig. 13: Error $e_i[\%]$ for all test sets and 10 sensors. All strains below 1e-5 are set to zero.

load applications are always somehow similar and just few mode shapes are dominant for vibrations that may occur.

3.7 Strain magnitude

An important criterion for feasibility is the magnitude of the strains that occur. Very small strains do not lead to any problems in the simulation, but are not measurable in reality. For further considerations, it is assumed that strains below 1e-5 are not measurable, between 1e-5 and 1e-4 are difficult to measure and greater than 1e-4 are easy to measure. In this section, the results are only discussed. Suggestions for improvements are made in the final section 4.

Table 2 holds some strain magnitudes for the selected sensors. One row represents one load case. The first row gives the strains if just the bolt load is acting. Since the bolts are not part of the model, the bolt strains were reconstructed according to the bolt load (50kN) and known data (M20, Young's modulus 210000N/mm^2). Row 2 to row 5 holds the data for the load cases which lead to the gap distributions given in Fig. 5. The last row contains the strain data for the load case which leads to the gap distribution depicted in Fig. 11.

If only the bolt load is acting, then only the strains in the bolts are easy to measure, all other strains remain very low. This suggests that the bolt strains have a dominant influence for the reconstruction of this load case. In this study, the assumption of uniform loads in all bolts was made. Given that the bolt load varies in real structures, it may be necessary to consider more, or even all bolts with strain gauges. As these are commercially available, the additional application effort is probably acceptable.

All other load cases in Table 2 either lead to leakage (rows 4 and 5) or are critical in this respect (rows 2, 3 and 6). In terms of the objectives of this work, they should be detectable. The data in Table 2 show that the critical loads in the longitudinal direction (rows 2 and 3) are easy to measure. The bending loads (rows 4 and 5) lead to some well measurable strains, to some that are at the limit of measurability and to not measurable strains. In order to estimate the influence of non-measurable strains, all strains smaller than 1e-5 were set to zero. The result can be seen in Fig. 13. Compared to Fig. 10, an increased but still acceptable error can be observed. The mean error increases from 2.5% to 3.9%. In only four of the 120 test cases does the error rise significantly above 10%. These are test cases 10, 55, 107 and 111. A closer look to the strain data shows that these are low-load test cases in which all strains are below 1e-4. The error of test cases 6, 24, 96 and 110 hardly changes at all. An inspection of the underlying strains shows that at least two values are higher as 1e-4 and good to measure. So if a critical load case is present and any strains are easily measurable, then the not measurable strains lose their significance. If all strains are small, this is not the case, but then, the flange should not be in a critical state. This assumption of less importance of small strains is underlined as well by the results of Section 3.8 where noisy strain data are used.

In summary, the following can be observed for the investigated structure: (1) The strains due to the bolt load are only measurable in the bolt strain gauges (2) With small additional loads, the gap can probably not be reconstructed

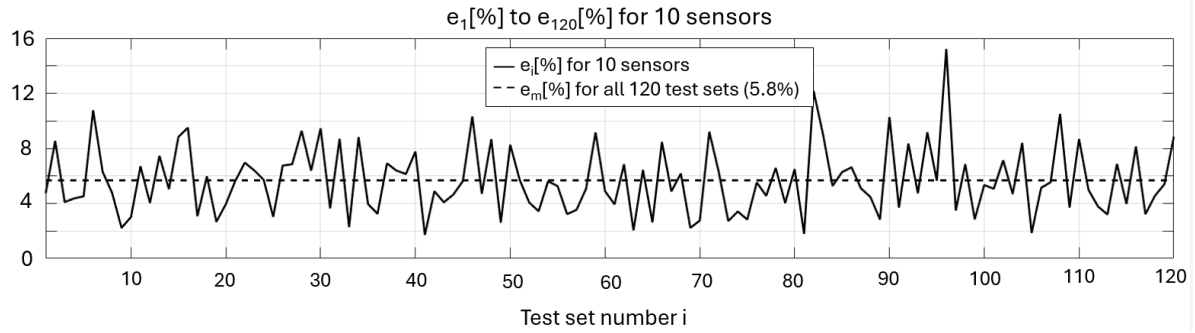

Fig. 14: Error $e_i[\%]$ for all test sets, 10 sensors and noisy strain data

accurately with real measurement data due to the inaccuracy of the strain gauges. (3) The strains have a measurable order of magnitude when the loads reach a critical range.

In any case, it would be better to measure higher strains values. In the presented example an unnecessary restriction has been introduced by the limitation of the potential sensor position next to the flange (see Fig. 2). Looking back, this was an intuitive decision which is questionable. Assuming that the gap distribution in the contact area is primarily influenced by global deformations or at least reacts quasi-statically to them, it would make more sense to consider the entire structure for the potential placement of sensors. Sensors placed away from the flange are certainly better suited to detect dominant load cases such as bending, torsion, or similar.

3.8 Noisy strain data

Real strain gauge data will always be influenced by noise. We investigated therefore the methods' robustness to noise by polluting the strain data. The starting point is the strains on which Fig. 10 is based. An equally distributed random number between -5% and +5% of the strain value has been added. Thus, only the result was polluted by noise, all underlying computations are the same as in Section 3.6.

The method without training data was extremely sensitive to noise, producing unusable results even with an equal number of sensors and modes.

However, the method using training data showed much better performance. As seen in Fig. 14, the results for the 120 test sets were still usable, although the error is higher compared to Fig. 10 where ideal data have been used. The mean error increases from 2.5% to 5.8%.

This brief investigation into noise suggests that the method with training data also appears to have a promising robustness against noise. Questions for future work could be to what extent the influence of noise depends on the number of contact modes and the number of strain gauges. The training data could also play a role in this regard insofar as the robustness to noise perhaps increases if noise is added to the training data.

4 Discussion, conclusion and outlook

The question posed at the beginning, namely whether a critical condition in the flange can be detected using a few strain measurements, can be answered with "Yes".

To answer this question, a virtual, model-based sensor was developed. It is based on contact modes and training data generated by simulations. Its application to a flange with 12 bores leads to the following conclusions and suggestions for improvement:

- The gap distribution in the contact area of a complex flange can be reconstructed with a few computed strains.
- The strains are within the measurable range, especially when the loads become critical.
- The results of the 120 test cases were robust against superimposed noise of 5% of the amplitude.
- For the gap reconstruction due to bolt load the strain gauges inside the bolts are crucial. It is probably advisable to apply strain gauges to all bolts. This likely makes sense because in reality not all bolts are loaded equally, as assumed here.

- Intuitively, we restricted potential sensor positions to the area of the flange. To measure larger and thus more noise-resistant strain values, it seems better to distribute potential sensor positions throughout the structure. This could be crucial for smaller and stiffer structures in order to obtain measurable strains.

The primary purpose of this work is to provide numerical evidence for the significance of strains in determining the state within a contact area. The next step would be an experimental application with measured strains. A few remarks on such an implementation are given in the following:

- Calibration could become a crucial aspect for a practical implementation. Potential reasons include, but are not limited to, imprecisely placed sensors, modeling inaccuracies, or non-perfectly flat surfaces. Static pressure films might be employed for calibration purposes. After applying a known load, the pressure film is removed and evaluated. Subsequently, the results can be used for calibration of a virtual and model-based sensor.
- Reconstructing the gap with a few strains is the most challenging task that can be posed. It is probably better to start with simpler questions. An example would be "Is the flange in a critical condition or not?". It is conceivable that machine learning can be used for such classifications instead of a model-based virtual sensor. If this is successful the issue of quantifying the gap can be addressed in a next step.

Authors' Contributions

Author 1 provided the basic idea, most of the theoretical considerations and the writing of the manuscript. Author 2 did all the practical work and computations during a master thesis. Author 3 supported the project in terms of practical help and consulting for theoretical questions.

References

[1] J. Lenz. *Strukturdynamik unter dem Einfluß von Mikro- und Markoschlupf in Fügestellen*. Ph.D. Thesis, Universität der Bundeswehr Hamburg, Fachbereich Maschinenbau, 1997.

[2] M. J. Kontoleon, E. S. Mistakidis, C. C. Baniotopoulos, and P. D. Panagiotopoulos. Parametric analysis of the structural response of steel base connections. *Computer and Structures*, 71:87 – 103, 1999.

[3] F. Pichler, W. Witteveen, and L. Koller. Efficient virtual tribomechadynamics by means of joint modes for detailed investigation of complex local stick and slip behavoiur in a joint. *Journal of Vibration and Acoustics*, 142, 2020. doi:10.1115/1.4047071.

[4] W. Witteveen, M. Kuts, and L. Koller. Can transient simulation efficiently reproduce well known nonlinear effects of jointed structures? *Mechanical Systems and Signal Processing*, 190, 2023. doi:10.1016/j.ymssp.2023.110111.

[5] M. Wall, M. S. Allen, and R. J. Kuether. Observations of modal coupling due to bolted joints in an experimental benchmark structure. *Mechanical Systems and Signal Processing*, 162, 2022. doi:10.1016/j.ymssp.2021.107968.

[6] S. Daouk, F. Louf, C. Cluzel, O. Dorival, L. Champaney, et al. Study of the dynamic behavior of a bolted joint under heavy loadings. *Journal of Sound and Vibration*, 392:307–324, 2017. doi:10.1016/j.jsv.2016.12.047.

[7] H. Bournine, D. J. Wagg, and S. A. Neild. Vibration damping in bolted friction beam-columns. *Journal of Sound and Vibration*, 330, 2011. doi:10.1016/j.jsv.2010.10.022.

[8] E. Jewell, M. S. Allen, I. Zare, and M. Wall. Application of quasi-static modal analysis to a finite element model and experimental correlation. *Journal of Sound and Vibration*, 479:115376, 2020. doi:10.1016/j.jsv.2020.115376.

[9] G. S. Li and Y. J. Chan. Visual investigation of static contact conditions at bolted joints. *International Journal of Solids and Structures*, 288:112621, 2024. ISSN 0020-7683. doi:10.1016/j.ijsolstr.2023.112621.

[10] T. Dreher, M. R. W. Brake, B. Seeger, and M. Krack. In situ, real-time measurements of contact pressure internal to jointed interfaces during dynamic excitation of an assembled structure. *Mechanical Systems and Signal Processing*, 160, 2021. doi:10.1016/j.ymssp.2021.107859.

[11] N. Chelimilla, V. Chinthapenta, N. Kali, and S. Korla. Review on recent advances in structural health monitoring paradigm for looseness detection in bolted assemblies. *Structural Health Monitoring*, 22(6), 2023. doi:10.1177/14759217231158540.

[12] T. Tong, J. Hua, F. Gao, and J. Lin. Identification of bolt state in lap joint based on propagation model and imaging methods of lamb waves. *Mechanical Systems and Signal Processing*, 200:110569, 2023. doi:10.1016/j.ymssp.2023.110569.

[13] B. He, B. Jiao, Q. Wan, R. Nie, and J. Yang. Strength and tightness evaluation method for pipe flange connectins considering thermal effects. *Journal of Lass Prevention in the Process Industries*, 83:105053, 2023. doi:10.1016/j.jlp.2023.105053.

[14] B. N. Khan, M. Abid, M. Jameel, and H. A. Wajid. Joint strength of gasketed bolted pipe flange joint under combined internal pressure plus axial load with different (industrial and asme) bolt-up strategy. *Proceedings of the Institution of Mechanical Engineers, Part E: Journal of Process Mechanical Engineering*, 231(3):555–564, 2017. doi:10.1177/0954408915614460.

[15] L. Zhu, A. H. Bouzid, and J. Hong. Numerical and experimental study of elastic interaction in bolted flange joints. *Journal of Pressure Vessel Technology*, 139(2):021211, 01 2017. doi:10.1115/1.4035316.

[16] L. Zhu, A. H. Bouzid, and J. Hong. Analytical evaluation of elastic interaction in bolted flange joints. *International Journal of Pressure Vessels and Piping*, 165:176–184, 2018. ISSN 0308-0161. doi:https://doi.org/10.1016/j.ijpvp.2018.06.012.

[17] L. Zhu, A. H. Bouzid, J. Hong, and Z. Zhang. Elastic interaction in bolted flange joints: An analytical model to predict and optimize bolt load. *Journal of Pressure Vessel Technology*, 140(4):041202, 06 2018. doi:10.1115/1.4040421.

[18] S. Chaturantabut and D. C. Sorensen. Nonlinear model reduction via discrete empirical interpolation. *SIAM Journal on Scientific Computing*, 32(5):2737–2764, 2010. doi:10.1137/090766498.

[19] P. Tiso and D. J. Rixen. Discrete empirical interpolation method for finite element structural dynamics. In *Topics in Nonlinear Dynamics, Volume 1, Vol. 35 of Conference Proceedings of the Society for Experimental Mechanics Series*, pages 203–212. Springer New York, New York, 2013.

[20] J. B. Rutzmoser. *Model Order Reduction for Nonlinear Structural Dynamics Simulation-free Approaches*. Ph.D. Thesis, Technical University Munich, Chair of Applied Mechanics, 2017.

[21] A. Chatterjee. An introduction to the proper orthogonal decomposition. *SIAM Journal on Scientific Computing*, 78(7):808–817, 2000, URL http://www.jstor.org/stable/24103957.

[22] G. Kerschen and J. C. Golinval. On the physical interpretation of proper orthogonal modes in vibrations. *Journal of Sound and Vibrations*, 211(4):607–616, 1998. doi:10.1006/jsvi.2001.3930.

[23] R. R. Craig and M. C. C. Bampton. Coupling of Substructures Using Component Modes. *AIAA Journal*, 3(4):678–685, 1968. doi:10.2514/3.4741.

[24] F. Pichler, W. Witteveen, and P. Fischer. A complete strategy for efficient and accurate multibody dynamics of flexible structures with large lap joints considering contact and friction. *Multibody System Dynamics*, 40(4):407–436, 2017. doi:10.1007/s11044-016-9555-2.

[25] J. H. Porter, N. N. Balaij, C. R. Little, and M. R. W. Brake. A quantitative assessment of the model form error of friction models across different interface representations for jointed structures. *Mechanical Systems and Signal Processing*, 163, 2022. doi:10.1016/j.ymssp.2021.108163.

[26] J. H. Porter and M. R. W. Brake. Towards a predictive, physics-based friction model for the dynamics of jointed structures. *Mechanical Systems and Signal Processing*, 192, 2023. doi:10.1016/j.ymssp.2023.110210.